Monthly Notices of the ROYAL ASTRONOMICAL SOCIETY

MNRAS **471,** 2438–2452 (2017) doi:10.1093/mnras/stx1673
Advance Access publication 2017 July 6

The SAMI Galaxy Survey: disc–halo interactions in radio-selected star-forming galaxies

S. K. Leslie,[1,2,3★] J. J. Bryant,[2,4,5] I.-T. Ho,[1,3,6] E. M. Sadler,[2,4] A. M. Medling,[1,7†] B. Groves,[1] L. J. Kewley,[1] J. Bland-Hawthorn,[4] S. M. Croom,[2,4] O. I. Wong,[8] S. Brough,[5] E. Tescari,[2,9] S. M. Sweet,[1] R. Sharp,[1] A. W. Green,[5] Á. R. López-Sánchez,[5,10] J. T. Allen,[2,4] L. M. R. Fogarty,[4] M. Goodwin,[5] J. S. Lawrence,[5] I.S. Konstantopoulos,[5,11] M. S. Owers[5,10] and S. N. Richards[2,4,5]

[1]*Research School of Astronomy and Astrophysics, Australian National University, Canberra, ACT 2611, Australia*
[2]*ARC Centre of Excellence for All-sky Astrophysics (CAASTRO), Canberra, Australia*
[3] *Max-Planck-Institut für Astronomie, Königstuhl 17, D-69117 Heidelberg, Germany*
[4]*Sydney Institute for Astronomy (SIfA), School of Physics, The University of Sydney, NSW 2006, Australia*
[5]*The Australian Astronomical Observatory, 105 Delhi Rd, North Ryde, NSW 2113, Australia*
[6]*Institute for Astronomy, University of Hawaii, 2680 Woodlawn Drive, Honolulu, HI 96822, USA*
[7]*Department of Astronomy, California Institute of Technology, 1200 E California Blvd, Pasadena, CA 91125, USA*
[8]*ICRAR-M468, University of Western Australia, 35 Stirling Highway, Crawley, WA 6009, Australia*
[9]*School of Physics, University of Melbourne, Parkville, VIC 3010, Australia*
[10]*Department of Physics and Astronomy, Macquarie University, NSW 2109, Australia*
[11]*Envizi Suite 213, National Innovation Centre, Australian Technology Park, 4 Cornwallis Street, Eveleigh, NSW 2015, Australia*

Accepted 2017 June 30. Received 2017 June 2; in original form 2016 December 13

ABSTRACT

In this paper, we compare the radio emission at 1.4 GHz with optical outflow signatures of edge-on galaxies. We report observations of six edge-on star-forming galaxies in the Sydney-AAO Multiobject Integral-field spectrograph Galaxy Survey with 1.4 GHz luminosities $>1 \times 10^{21}$ W Hz^{-1}. Extended minor axis optical emission is detected with enhanced [N II]/Hα line ratios and velocity dispersions consistent with galactic winds in three of six galaxies. These galaxies may host outflows driven by a combination of thermal and cosmic ray processes. We find that galaxies with the strongest wind signatures have extended radio morphologies. Our results form a baseline for understanding the driving mechanisms of galactic winds.

Key words: cosmic rays – galaxies: evolution – galaxies: haloes – galaxies: ISM – galaxies: jets – galaxies: kinematics and dynamics.

1 INTRODUCTION

Galactic winds, driven by star formation or active galactic nuclei (AGNs), are arguably the most important feedback processes in galaxy formation and evolution (Veilleux, Cecil & Bland-Hawthorn 2005). Without incorporating outflows, galaxy formation models predict galaxy star formation rates (SFRs) much higher than those observed; large-scale outflows remove gas content and therefore suppress the SFRs of galaxies (e.g. Cole et al. 2000; Springel & Hernquist 2003; Kereš et al. 2009 and references therein). Outflows from galaxies also drive metal-enriched gas out into the surrounding medium and are therefore thought to be responsible for the heavy elements present in the circumgalactic medium (Tumlinson et al. 2011; Werk et al. 2013). Galactic winds are ubiquitous in local galaxies with a high SFR surface density (>0.1 M$_\odot$ yr^{-1} kpc^{-2}), with outflow velocities seemingly correlated with specific SFR ($\dot{M}/M_*$; Heckman, Armus & Miley 1990; Grimes et al. 2009) or circular velocity (e.g. Heckman et al. 2015). The discovery of powerful winds in high-redshift galaxies (e.g. Pettini et al. 2000; Steidel et al. 2010; Genzel et al. 2011; Newman et al. 2012; Genzel et al. 2014) further implicates wind-related feedback processes as key to the chemical and thermal evolution of galaxies and the intergalactic medium.

The galactic fountain model of Shapiro & Field (1976) describes how outflows with velocities less than the escape velocity will eventually fall back on to the galactic disc, resulting in the circulation of matter through disc–halo interactions. Disc–halo interactions include outflows from star-forming regions (Normandeau, Taylor & Dewdney 1996) and cool clouds falling back into the disc from the halo (Pietz et al. 1996). The chimney model of Norman & Ikeuchi

★ E-mail: sarah@mso.anu.edu.au
† Hubble Fellow.

© 2017 The Authors
Published by Oxford University Press on behalf of the Royal Astronomical Society

Downloaded from https://academic.oup.com/mnras/article-abstract/471/2/2438/3930853/The-SAMI-Galaxy-Survey-disc-halo-interactions-in
by California Institute of Technology user
on 21 September 2017

(1989) suggests more localized outflows than the fountain model. Neutral hydrogen supershells are driven by stellar winds and supernova activity and leave relative 'holes' where the stars were. If the supershells are sufficiently energetic, they can break through the gas layers of the disc, resulting in a chimney-shaped structure. Such chimneys would provide an unobstructed route for photons to escape the disc and ionize gas at large scaleheights. Magnetic fields would also follow these chimneys or filaments, allowing cosmic rays (CRs) to be more easily advected into the halo.

CRs provide an important additional pressure on the gas, thereby helping to drive gas into the halo. Recent simulation papers such as Uhlig et al. (2012), Booth et al. (2013), Salem & Bryan (2014), Girichidis et al. (2016), Simpson et al. (2016), Ruszkowski, Yang & Zweibel (2017) and Wiener, Pfrommer & Oh (2017) explore the importance of CRs in driving winds in star-forming galaxies. CR-driven winds are able to explain outflows with a low velocity ($\sim$20 km s^{-1}) and correspondingly low-SFR surface densities (below 0.1 $M_\odot$ yr^{-1} kpc^{-2}). CR energy is not dissipated as fast as thermal energy. CR pressure is able to act over larger distances than thermal pressure, thus helping to drive winds where a thermal wind alone would fail (Everett et al. 2008). On the other hand, CR pressure is relatively inefficient at driving winds from the galactic mid-plane compared to gas pressure when the wind is sub-Alfvénic (Everett et al. 2008). Thus, a mixture of thermal pressure, to efficiently launch the wind and CR pressure, to efficiently drive the wind to large radii, would be desirable for expelling gas from a galaxy.

Edge-on galaxies provide the best view of extraplanar gas at the interface between a galaxy disc and halo. Observations of nearby edge-on galaxies show that gas, dust and CRs exist above and below the disc (Beuermann, Kanbach & Berkhuijsen 1985; Popescu et al. 2004; Madsen & Reynolds 2005; Irwin & Madden 2006). Hα narrow band imaging has revealed strong starburst-driven winds in galaxies such as M82 (Axon & Taylor 1978; Bland & Tully 1988) and NGC 253 (Westmoquette, Smith & Gallagher 2011), which have bipolar structures centred on a central starburst and extending several kiloparsecs in disc height. Studies have also revealed that extended diffuse emission and filamentary structures are common in nearby galaxies: More than 50 per cent of galaxies have extraplanar diffuse emissions from 1–2 kpc to even 4 kpc above the disc (Rossa & Dettmar 2000, 2003; Miller & Veilleux 2003). However, haloes are intrinsically faint (low surface brightness) emitters, rendering them hard to detect (e.g. Hummel, Beck & Dahlem 1991).

Radio continuum emission that extends along the minor axis of edge-on spiral galaxies to form a 'thick disc' has been detected in nearby galaxies such as NGC 4565, NGC 5909 (Hummel, van Gorkom & Kotanyi 1983), NGC 5775 (Duric, Irwin & Bloemen 1998), NGC 3044 (Sorathia 1994) and NGC 3556 (Bloemen, Duric & Irwin 1993). Krause (2012) measured the vertical scaleheights of the radio emission at 6 cm for five edge-on galaxies and found they all had similar vertical scaleheights for the thin and thick discs, with a mean thick-disc scaleheight of 1.8 ± 0.2 kpc. X-shaped magnetic fields in the thick disc/halo were also detected for eight edge-on galaxies spanning a range of Hubble types and SFRs 0.6 $M_\odot$ yr^{-1} $\leq$ SFR $\leq$ 7.3 $M_\odot$ yr^{-1} (Krause 2012). The strength of the X-shaped fields can be explained by models including a galactic wind (Krause 2012). Biconical outflows were also predicted by the CR-driven models of Salem & Bryan (2014).

At optical wavelengths, high-resolution spectroscopy can be used to identify shocks from galactic winds in galaxies (Veilleux et al. 2005). Emission-line ratios typical of shock excitation (e.g. [N II]/H$\alpha > 1$) indicate winds in the absence of AGN activity. Studies of local galaxies show that outflows are usually associated with interstellar shocks that excite optical line emission, enhancing line ratios such as [N II]/Hα, [S II]/Hα and [O I]/Hα (Rich et al. 2010; Rich, Kewley & Dopita 2011; Soto & Martin 2012; Soto et al. 2012). For inclined galaxies, one can use the excitation contrast in the shock-excited wind material and the star-forming disc to search for and detect galactic winds (e.g. Veilleux & Rupke 2002). Samples of a few tens of galactic wind galaxies have been studied using slit spectroscopy and narrow-band imaging (e.g. Heckman et al. 1990; Veilleux et al. 2003, 2005).

Integral field spectroscopy (IFS) is an ideal tool for investigating galactic winds, allowing spatially resolved kinematic and excitation information to be obtained simultaneously. The use of optical diagnostic diagrams with spatially resolved data can allow the separation of winds driven by starbursts from those driven by AGNs (Sharp & Bland-Hawthorn 2010). Therefore, IFS of highly inclined galaxies is an excellent method for identifying wind signatures in star-forming galaxies and studying disc–halo interactions in more detail.

We draw optical IFS data from an on-going multiplexed integral field unit (IFU) survey: the Sydney-AAO Multi-object Integral-field spectrograph (SAMI) Galaxy Survey (Croom et al. 2012; Bryant et al. 2015). The ability of SAMI to detect galactic winds in star-forming galaxies has already been demonstrated by Fogarty et al. (2012) and Ho et al. (2014). The high spectral resolution of SAMI ($R \approx 4500$ in the red arm) allowed Ho et al. (2014) to decompose the spectral lines from a moderately inclined disc galaxy ($i = 43^\circ$) into three separate kinematic components having different velocities, velocity dispersions and line ratios; one of the components traced a bipolar outflow. A sample of 40 star-forming edge-on galaxies in the SAMI survey was studied by Ho et al. (2016b). Ho et al. (2016b) found large-scale winds preferentially in galaxies with high-SFR surface densities and recent bursts of star formation.

Low-frequency (1.4 GHz) radio observations are sensitive to the synchrotron emission resulting from CR electrons in the presence of a magnetic field. Using radio images from the Faint Images of the Radio Sky at Twenty-centimetres (FIRST) survey, we can test which conditions enable CRs to escape to the largest disc heights. Following the work of Ho et al. (2016b), we discuss six edge-on star-forming galaxies in the SAMI Galaxy Survey that show evidence for low-velocity outflows and have strong radio continuum emission.

The paper is structured as follows. In Section 2 we discuss our sample selection, detail our observations, data reduction and spectral analysis. We analyse emission-line ratio maps, velocity and velocity dispersion maps in Section 3. We also employ the gas kinematic classification developed in Ho et al. (2016b) to identify wind-dominated galaxies. In Section 4, we present the FIRST maps of the galaxies and discuss the extent of the radio emission and the location of our sample with respect to the radio–far-infrared relation. We discuss our results in the context of disc–halo interactions in Section 5. Finally, we give our conclusions in Section 6.

Throughout this paper, we assume a $(h, \Omega_m, \Omega_\Lambda) = (0.7, 0.3, 0.7)$ Cosmology and a Salpeter initial mass function.

2 SAMPLE

2.1 SAMI Galaxy Survey data

To investigate disc–halo interactions in star-forming galaxies, we identify edge-on galaxies observed by the SAMI Galaxy Survey that have measured radio continuum emission. The SAMI Galaxy Survey covers a broad range in stellar mass and environment. Full

Downloaded from https://academic.oup.com/mnras/article-abstract/471/2/2438/3930853/The-SAMI-Galaxy-Survey-disc-halo-interactions-in
by California Institute of Technology user
on 21 September 2017

Table 1. Information from the GAMA second public data release and on the SAMI observations of the six galaxies in our sample.

ID	GAMA ID	RA	Dec.	z	r_e^a (arcsec)	i^b (deg)	$\log(\frac{M_*}{M_\odot})^c$	SFR^d ($M_\odot$ yr^{-1})	Date Obs ^{e}	FWHM^f (arcsec)
1	551202	09:17:28.99	−00:37:14.1	0.0165	12.69	78.5	9.967	4.59	2014 April 04	1.85
2	417678	08:50:57.17	+02:20:46.2	0.0405	4.33	90.0	10.11	10.13	2014 April 06	2.29
3	593680	14:29:46.05	−00:09:08.6	0.0300	11.53	90.0	10.411	1.90	2013 April 14 and 16	2.18
4	600030	08:53:58.68	+00:21:00.1	0.0292	8.27	73.0	10.237	5.10	2013 March 13	1.60
5	376293	08:51:11.41	+01:30:06.1	0.0605	6.96	82.2	10.65	2.25	2015 January 25	2.72
6	227607	14:17:17.86	+01:09:22.4	0.0545	10.69	76.0	10.75	2.30	2015 May 23	1.61

^{a}Effective radii and ^{b}inclination angle from the r-band photometry (Kelvin et al. 2012). ^{c}GAMA stellar masses ($M\star/M_\odot$) (Taylor et al. 2011). ^{d}GAMA Hα star formation rates (Hopkins et al. 2013). ^{e}The date(s) the target was observed with SAMI. ^{f}The effective seeing of the SAMI observation.

details of the target selection can be found in Bryant et al. (2015). Briefly, the SAMI Galaxy Survey includes four volume-limited samples based on pseudo-stellar mass cuts all selected from the Galaxy and Mass Assembly (GAMA) project (Driver et al. 2011). To extend the survey sample to high-density environments, eight clusters with virial masses $>10^{14}$ $M_\odot$ are also targeted by the survey (Owers et al. 2017). SAMI–GAMA targets cover $0.004 < z < 0.095$, Petrosian r-band magnitudes < 19.8 and a stellar mass range of 10^7–10^{12} $M_\odot$. The GAMA regions were selected because of the deep spectroscopy down to $r < 19.8$ mag of ∼300 000 galaxies, and the vast array of ancillary data available, including *ugrizYJHK* images through to radio bands.

IFS observations were performed using SAMI (Croom et al. 2012) and are described in Table 1. SAMI is mounted at the prime focus on the Anglo-Australian Telescope that provides a 1 deg diameter field of view. SAMI uses 13 fused fibre bundles (hexabundles, Bland-Hawthorn et al. 2011; Bryant et al. 2011, 2014) with a high (75 per cent) filling factor. Each bundle contains 61 fibres of 1.6 arcsec diameter resulting in each IFU having a diameter of 15 arcsec. The IFUs, as well as 26 sky fibres, are plugged into pre-drilled plates using magnetic connectors. SAMI fibres are fed to the double-beam AAOmega spectrograph (Sharp et al. 2006). The SAMI Galaxy Survey uses the 570 V grating at 3700–5700 Å giving a resolution of $R = 1730$ ($\sigma = 74$ km s^{-1}) and the 1000R grating from 6250 to 7350 Å giving a resolution of $R = 4500$ ($\sigma = 29$ km s^{-1}).

The data were reduced using the SAMI data reduction pipeline described in Sharp et al. (2015), Allen et al. (2015) and Green et al. (in preparation). Final SAMI data products are sampled to a grid with square pixels 0.5 arcsec wide.

The seeing conditions of our observations are measured from reduced data cubes of a calibration star observed simultaneously with the science targets. As described in Allen et al. (2015), the spatial point spread function (PSF) of the SAMI data cubes is primarily determined by the atmospheric conditions at the Anglo-Australian Telescope. A 2D Moffat distribution was fit to the red cube of the calibration stars to provide an estimate of the seeing disc. We note that the PSF profile is a function of wavelength, with larger seeing disks on average towards the blue. We report the full width at half-maximum (FWHM) of the resulting fits in Table 1.

2.2 First radio data

To investigate the relationship between CR electrons and their host galaxies, we select SAMI targets that have strong 1.4 GHz radio continuum emission. Synchrotron emission from the CR electrons in a galaxy will dominate the radio emission of star-forming galaxies at frequencies lower than ∼30 GHz (Condon 1992). The non-thermal synchrotron component comprises ∼90 per cent of the radio emission at 1.4 GHz for star-forming galaxies (Condon 1992). CRs can travel 1–3 kpc during their lifetime in a galaxy disc or filament, respectively (Collins et al. 2000). Detecting CRs at heights >3 kpc above a galaxy disc could be an indication of a galactic wind or chimney.[1] We draw radio continuum data from the FIRST (Becker, White & Helfand 1995) survey, a 1.4 GHz continuum survey carried out by the National Radio Astronomy Observatory (NRAO) with the Very Large Array (VLA). The FIRST survey was conducted in the B-configuration of the VLA, and thus has a resolution of ∼5.4 arcsec. At the 1 mJy source detection threshold, the survey is 80 per cent complete and has ∼90 sources per square degree, ∼35 per cent of which have resolved structure on scales from 2 to 30 arcsec. A publicly available source catalogue[2] includes peak and integrated flux densities and sizes derived from fitting a two-dimensional Gaussian profile to each source. The astrometric uncertainty of the sources is 1 arcsec.

2.3 Cross-matched sample

We positionally cross-matched potential SAMI targets with radio surveys FIRST and NVSS (NRAO VLA Sky Survey; Condon et al. 1998). Radio contours were overlaid on optical images to visually confirm matches. We find that ∼4 per cent of the 5546 potential SAMI targets in the GAMA regions have associated radio sources in either survey, with approximately two thirds of these being optically classified as star forming using the Kewley et al. (2001) classification and GAMA single fibre spectroscopy (Hopkins et al. 2013).

Due to sensitivity limits, FIRST primarily detects luminous galaxies with radio SFRs $\gtrsim 1$ $M_\odot$ yr^{-1}, that corresponds to galaxies more massive than $10^{9.5}$ $M_\odot$. The FIRST catalogue only contains galaxies with a high surface brightness, likely biasing our radio-selected sample towards a larger fraction of wind-dominated galaxies, because wind activity is thought to correlate with SFR surface density (Heckman et al. 1990; Ho et al. 2016b).

2.4 Selection criteria

Galaxies dominated by AGNs were removed from the sample using the GAMA spectra (Liske et al. 2015) or central SAMI spectra which probes the central 2 arcsec of the galaxies and the Kewley et al. (2006) classification scheme. However, some radio AGNs do

[1] The presence of a radio jet can also result in radio emission >3 kpc away from a galaxy disc. Jets and galactic winds can be differentiated via their radio morphology.
[2] http://sundog.stsci.edu/first/catalogs.html

Downloaded from https://academic.oup.com/mnras/article-abstract/471/2/2438/3930853/The-SAMI-Galaxy-Survey-disc-halo-interactions-in
by California Institute of Technology user
on 21 September 2017

not show strong optical AGN signatures (Ivezić et al. 2002; Sadler et al. 2002), so the removal of optically luminous AGNs does not necessarily mean that our sample is free of radio AGNs. Thirty star-forming galaxies, observed with SAMI as of 2016 June, remain after removing AGN-host galaxies.

For our analysis of disc–halo interactions, we make cuts on galaxy size and inclination. Effective radii (r_e) and ellipticity were measured from Sérsic profile fits to reprocessed SDSS (Sloan Digital Sky Survey; York et al. 2000; Stoughton et al. 2002) *r*-band images by the GAMA team (Kelvin et al. 2012). To observe gas excitation above and below the disc, we require the galaxy effective radius to be less than the size of the SAMI IFUs, 15 arcsec (this excludes one galaxy, GAMA 204799). Galaxy inclination is determined using the galaxy minor-to-major axis ratio, b/a. We apply a cut to only include edge-on galaxies using the criteria $\frac{b}{a} \leq 0.35$. This corresponds to an inclination angle $i = 73^\circ$ calculated using the Hubble (1926) formula:

$$\cos^2(i) = \frac{(\frac{b}{a})^2 - q_0^2}{1 - q_0^2},$$

where $q_0 = 0.2$ is related to the intrinsic flattening of the distribution of light of galactic spheroids. Additionally, GAMA 504713 was excluded from the analysis due to the poor fit of a single-Sérsic profile to the *r*-band photometry ($\chi^2 \approx 2$).

2.5 The sample

Our selection resulted in a sample of six edge-on, star-forming, radio continuum detected galaxies for which CR pressure could play an important role in driving disc–halo interactions. The six nearby edge-on galaxies in our sample, with GAMA catalogue identifications 551202, 417678, 593680, 600030, 376293 and 227607 (which we will refer to hereafter as Galaxies 1–6, respectively) are shown in Fig. 1. Row A contains SDSS *gri* composite images with the SAMI hexabundle field of view (15 arcsec in diameter) overlaid. The dust lanes and stellar bulges of Galaxies 1, 3, 4, 5 and 6 can be seen in the optical images.

2.6 Spectral analysis

We use the spectral fitting pipeline LZIFU (Ho et al. 2016a) to extract the emission-line fluxes and kinematic information from the SAMI data cubes for each galaxy. On a spaxel-by-spaxel basis, the continuum is modelled and subtracted and the emission lines are fit to the resulting spectrum. LZIFU uses the penalized-pixel fitting routine (PPXF; Cappellari & Emsellem 2004) to model the continuum spectrum using spectral synthesis models. We use templates from González Delgado et al. (2005) made with Padova stellar evolutionary tracks, three metallicities, $Z = 0.004$, 0.008 and 0.019 (solar), and 24 ages ranging from 0.004 to 11.220 Gyr. Once the continuum is subtracted, we fit 11 strong optical lines simultaneously: [O II] 3726,29, H β, [O III] 4959,5007, [O I] 6300, [N II] 6548,84, H α and [S II] 6716,31. Emission lines are fitted with a single Gaussian component at each spaxel using the MPFIT package, which performs a least-squares analysis using the Levenberg-Marquardt algorithm (Markwardt 2009). The ability of LZIFU to fit multiple Gaussian components to the emission-line spectra is most useful where any outflowing component would be superimposed along our line of sight with the disc, such as for a face-on galaxy. For our edge-on sample, a one-component fit was preferred to a two-component Gaussian fit in the extraplanar regions based on the *F*-test and confirmed through visual inspection. We thus use LZIFU to only fit a single Gaussian per emission line. Spaxels located outside of one effective radius have mean reduced $\chi^2 \leq 1$ for all six galaxies (reduced $\chi^2 = 0.919$, 1.11, 0.905, 0.935, 0.965, 0.963 for galaxies 1–6, respectively). By fitting all lines simultaneously, every line is constrained to share the same velocity and velocity dispersion.

The H α flux maps of all six galaxies are shown in row B of Fig. 1. The H α emission traces the recent (<10 Myr) star formation activity (but it also suffers from dust extinction).

3 OPTICAL SIGNATURES OF DISK–HALO INTERACTIONS

In this section, we present our analysis of the emission line and gas kinematic properties of our galaxies.

3.1 Emission-line ratio maps

We examine maps of the [S II] λ6716,31 doublet (hereafter [S II]) to H α flux ratio in row C of Fig. 1 as a first step towards understanding the processes at work in the galaxies. The [S II]/H α ratio is sensitive to metallicity and ionization parameter (Denicoló, Terlevich & Terlevich 2002; Kewley & Dopita 2002; Pettini & Pagel 2004; Kewley & Ellison 2008) and has the advantage of not requiring reddening corrections. The [S II]/H α ratio can be excited by interstellar shocks (e.g. Shull & McKee 1979; Farage et al. 2010; Rich et al. 2010). All six galaxies show the same trend: above and below the disc, the [S II]/H α ratio increases. Higher ratios in the outer regions usually correspond to shocked regions, as seen by Veilleux & Rupke (2002), Rich et al. (2010), Monreal-Ibero, Arribas & Colina (2006), Sharp & Bland-Hawthorn (2010), Rich et al. (2011) and Fogarty et al. (2012).

The [N II]/H α line ratios and [O I]/H α line ratio (see Figs 2 and 3) also follow the same trend as the [S II]/H α maps, with line ratios increasing with distance from the disc for all six galaxies.

Spiral galaxies with a layer of vertically extended diffuse ionized gas (eDIG) also show a rise in [N II]/H α and [S II]/H α. Diffuse ionized gas is a warm (10^4 K), low density (10^{-1}cm^{-3}), ionized medium, known in our own galaxy as the Reynolds layer (Reynolds 1993). There is a lack of consensus in the literature on how to explain the emission properties of eDIG (Domgorgen & Mathis 1994; Veilleux, Cecil & Bland-Hawthorn 1995; Bland-Hawthorn, Freeman & Quinn 1997; Rand 1998; Otte & Dettmar 1999; Tüllmann & Dettmar 2000). The ionization state of eDIG is generally compatible with the ionizing flux from stellar sources (O and B stars), hardened by photoelectric absorption (Hoopes & Walterbos 2003; Rossa & Dettmar 2003; Oey et al. 2007; Haffner et al. 2009; Blanc et al. 2009). However, some observations could be more consistent with shocks (Shull & McKee 1979), turbulent mixing layers (Slavin, Shull & Begelman 1993) or CR heating (Hartquist & Morfill 1986; Parker 1992).

Increased [S II]/H α and [N II]/H α ratios could be explained by increasing the ionization parameter in pure photoionization models. However, the [S II]/[N II] ratio is sensitive to the ionization parameter, and consequently would be required to decrease with disc height (Rand 1998; Domgorgen & Mathis 1994; Bland-Hawthorn et al. 1997). We show the [S II]/[N II] line ratios for our six galaxies in row G of Fig. 1. Only spaxels with signal-to-noise ratio (S/N) >5 in both lines have been included. In the case of Galaxies 4–6, the signal-to-noise cut removes most of the extraplanar emission. However, the [S II]/[N II] ratio is not seen to decrease with disc height, which would be required if a change in ionization parameter was causing the increased [S II]/H α and [N II]/H α observed. In the

Downloaded from https://academic.oup.com/mnras/article-abstract/471/2/2438/3930853/The-SAMI-Galaxy-Survey-disc-halo-interactions-in
by California Institute of Technology user
on 21 September 2017

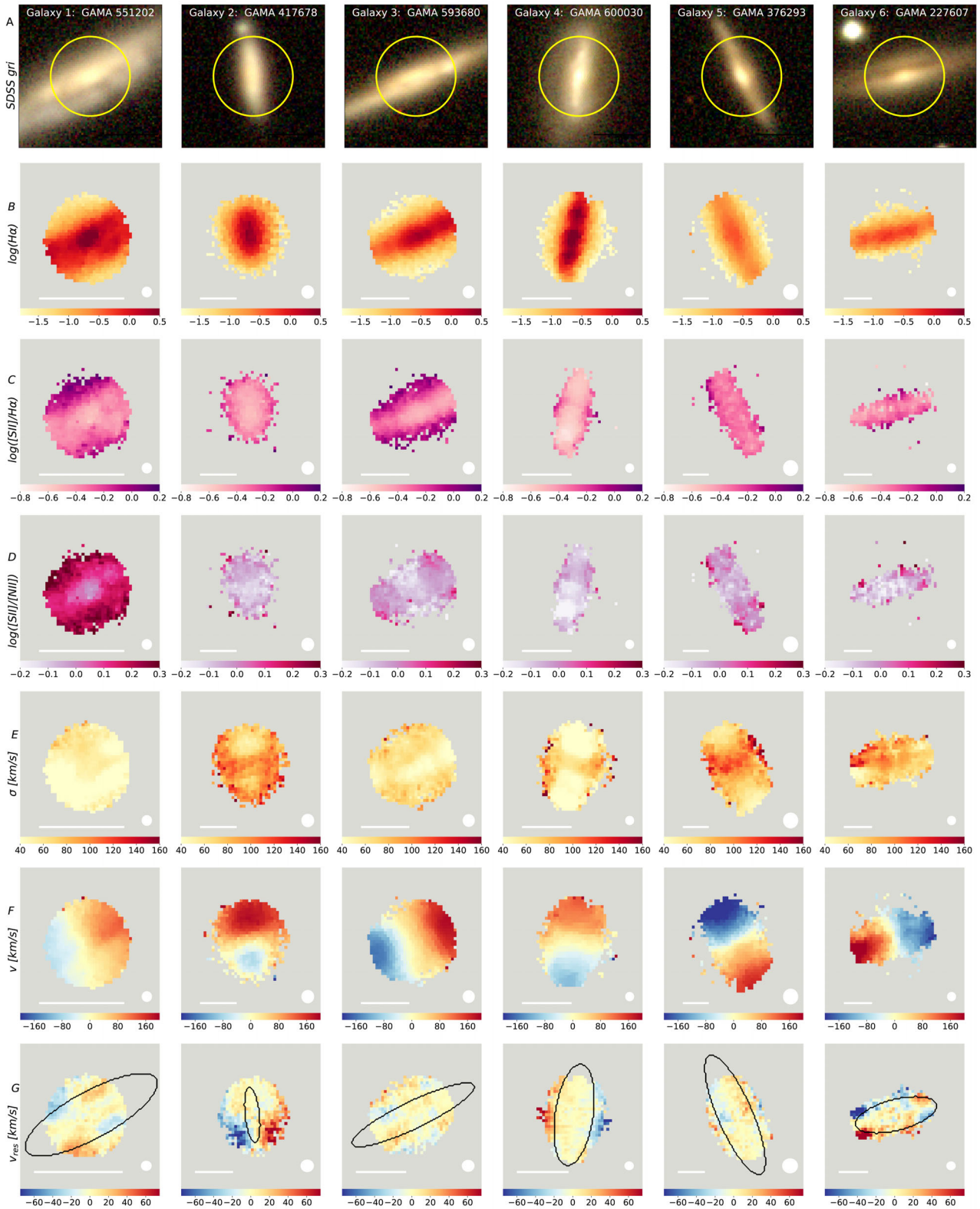

Figure 1. Each column represents the properties of one galaxy. Row A shows $1' \times 1'$ SDSS *g r i* composite images with the SAMI hexabundle field of view (15 arcsec in diameter) overlaid. Row B shows the log of the total Hα flux (in units of 10^{-16} erg s^{-1}cm^{-2}). Row C shows maps of log([S II]/Hα). In all six galaxies, the line ratios increase with distance from the disc. Row D shows maps of log([S II]/[N II]). Row E shows maps of velocity dispersion, σ (in km s^{-1}). Row F shows velocity maps (in km s^{-1}). All galaxies show clear signs of rotation. Row G shows velocity residual maps, obtained by reflecting the velocity field about the major axes and subtracting the reflected map from the original map shown in row F. Black ellipses represent one effective radius padded by 1 arcsec, $\tilde{r_e}$). In all panels, only spaxels with S/N $\geq$ 5 in relevant properties are shown. White bars at the bottom of the maps of SAMI data indicate 5 kpc in projection at the redshift of each galaxy. The effective seeing disc of each observation is represented by a white circle at the bottom right of the maps.

Downloaded from https://academic.oup.com/mnras/article-abstract/471/2/2438/3930853/The-SAMI-Galaxy-Survey-disc-halo-interactions-in
by California Institute of Technology user
on 21 September 2017

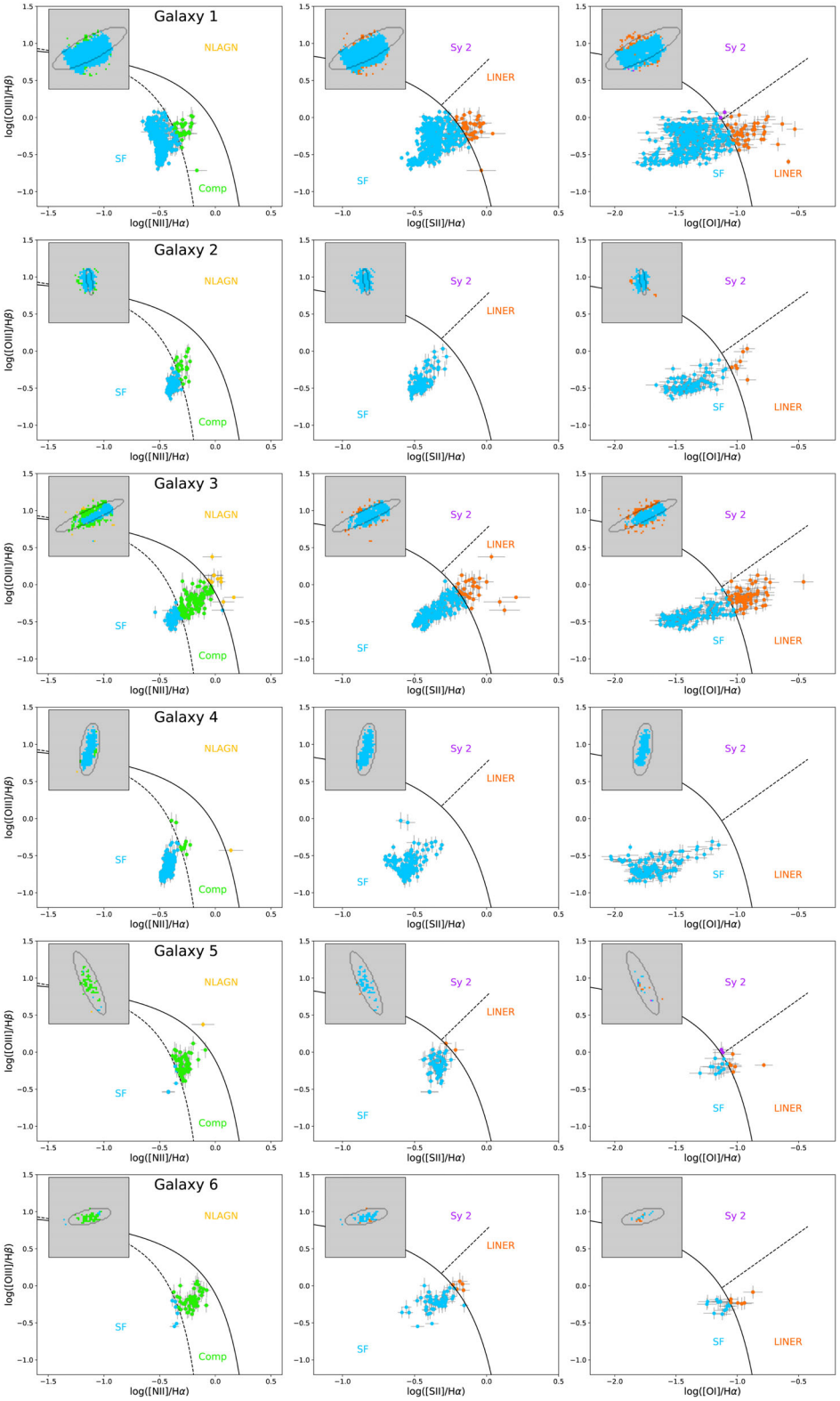

Figure 2. Emission-line ratio diagnostic diagrams of each spaxel in each galaxy. Black solid curves form an upper limit for star-forming galaxies as derived by Kewley et al. (2001). The dashed line on the [N II] diagram is the empirical Kauffmann et al. (2003) boundary below which galaxies are classified as star-forming. The dashed lines on the [S II] and [O I] diagrams were derived by Kewley et al. (2006) to empirically separate Seyfert 2 galaxies and LINERs. In the leftmost panel, NLAGN represents narrow emission-line AGNs (Seyfert 2 plus LINERs); Comp represents starburst–AGN composites. We apply a minimum S/N cut of 5 in every diagnostic line. The spaxels in each diagram reflect a mix of ionization sources, with spaxels branching from the star-forming regions to the LINER/shocked regions on the diagrams. The insets map the location of the spaxels included in each diagnostic diagram with the same colour coding as their respective diagram. Ellipses show r_e as determined from the *r*-band photometry.

Downloaded from https://academic.oup.com/mnras/article-abstract/471/2/2438/3930853/The-SAMI-Galaxy-Survey-disc-halo-interactions-in
by California Institute of Technology user
on 21 September 2017

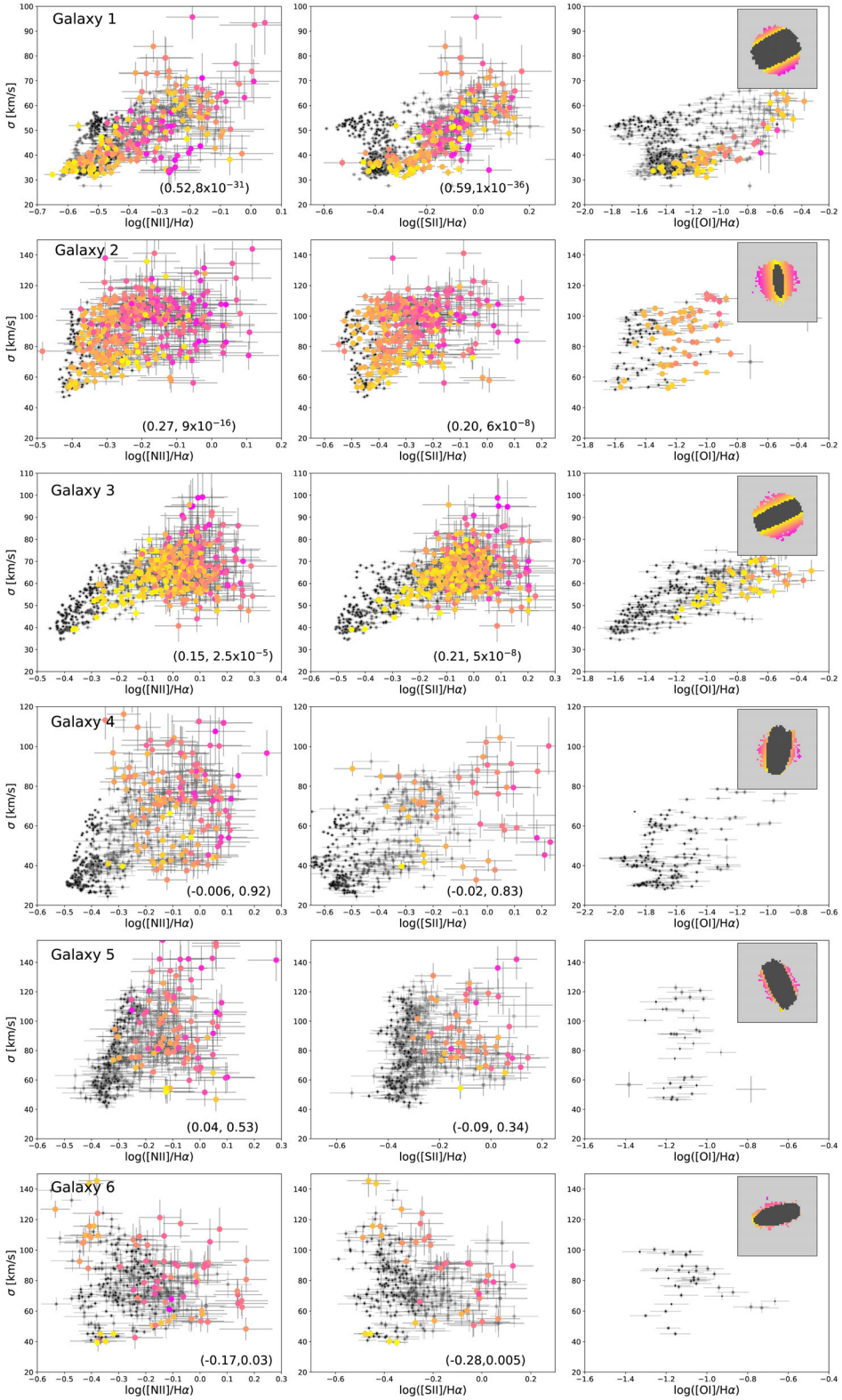

Figure 3. Relationship between log([N II]/H α), log([S II]/H α) and log([O I]/H α) and velocity dispersion for the six galaxies. All spaxels with signal-to-noise ratio greater than five in relevant properties, H α, velocity dispersion and either [N II], [S II] or [O I], are considered here. Spaxels greater than 1 $\tilde{r_e}$ are colour coded by disc height (as mapped in the inset), which is calculated using the exponential fits to the *r*-band images by the GAMA team. Spaxels with distances $< \tilde{r_e}$ are considered to belong to the galaxy disc and are coloured dark grey. Kendall's tau correlation coefficient and significance values were calculated to assess the correspondence between line ratio and velocity dispersion for spaxels outside 1 $\tilde{r_e}$ and they written in the bottom right corner of the [N II]/H α and [S II]/H α panels. For galaxies 1–3, there is a significant positive correlation between line ratio and velocity dispersion in the extra-planar gas. We suggest this is due to shocks, which cause higher line ratios and velocity dispersions in the emission-line gas than star formation alone.

Downloaded from https://academic.oup.com/mnras/article-abstract/471/2/2438/3930853/The-SAMI-Galaxy-Survey-disc-halo-interactions-in
by California Institute of Technology user
on 21 September 2017

centre of Galaxy 3, there is a decrease in [S II]/[N II] ratio which corresponds to an increase in ionization parameter. This region is biconical in shape and could be due to shocked outflowing gas. A similar, although less pronounced, decrease in the central line ratios for Galaxies 6 and 2 is also seen. There is an unusual partially resolved region in Galaxy 4 with low [S II]/[N II] ratio (high ionization parameter), spatially coincident with an H II region (as traced by H α). This region could correspond to recent star formation and supernovae activity. The varying [S II]/[N II] ratio in the galaxies in our sample suggests that the enhanced extraplanar emission-line ratios are not caused by photoionization alone.

3.2 Optical diagnostic diagrams

Line ratios such as [N II]/H α, [S II]/H α, [O I]/H α and [O III]/H β are sensitive to the hardness of the ionizing radiation field and therefore provide key diagnostics of the ionizing power sources in a galaxy. Diagnostic diagrams using these ratios were first employed by Baldwin, Phillips & Terlevich (1981) and Veilleux & Osterbrock (1987) to classify the dominant energy source of a galaxy. These standard optical diagnostic diagrams for the six galaxies in our sample are shown in Fig. 2. We include emission-line fluxes with S/N $>$ 5 in all relevant lines. In all three diagnostic diagrams, emission due to photoionization by H II regions results in line ratios which lie on the lower-left hand side of the diagrams. The observed dashed curve in the [N II] diagnostic separates purely star-forming objects (below the curve) from composite objects containing both star formation and Seyfert 2/LINER-like activity and was derived by Kauffmann et al. (2003) using the SDSS sample. The dashed line on the [S II]/H α and [O I]/H α diagnostics represents an empirically derived boundary between Seyfert 2s and LINERs (Kewley et al. 2006). Shock excitation can cause enhanced line ratios, moving the diagnostic towards the LINER region (Rich et al. 2010, 2011). Insets in Fig. 2 show maps of the classification regions, made using the same colour coding as the data in the diagrams.

All six galaxies have spaxels lying near the purely star-forming region, as well as spaxels branching into the composite region. Galaxy 1 shows data consistent with an abundance sequence following the curve from high [O III]/H β and low [N II]/H α, corresponding to low abundances, to regions of lower [O III]/H β and higher [N II]/H α consistent with higher abundances. The galaxy also shows evidence for a second branch where both [O III]/H β and [N II]/H α increase together, and also with the disc height as shown in the inset. This second trend can be interpreted as a shock mixing sequence, with shock excitation having an increasing contribution to the emission with increasing line ratios. Galaxy 4 also shows evidence for both star-forming and shock mixing sequences, particularly in the [S II] diagnostic, as does Galaxy 6. Galaxies 2 and 3 show evidence for a single sequence of shock mixing. Extended LINER-like emission-line ratios can be explained by shock models (Allen et al. 2008; Rich et al. 2010, 2011); however, they could also be due to other mechanisms such as hot evolved post-AGB stars (see Belfiore et al. 2016 and references therein). Based on the stacking analysis of Ho et al. (2016a) (see their figs 12–14), we believe the increase in emission-line ratios with galaxy disc height is a true behaviour in galaxies 1–3, not an artefact of our S/N cut. The composite and LINER-like emission ratios in the galactic winds in galaxies 1–3 can be explained by wind activity causing shock excitation.

A limiting factor in the optical diagnostic diagrams is the low S/N of the [O III]/H β ratio. In Fig. 3, we compare the [N II]/H α, [S II]/H α and [O I]/H α line ratios to their corresponding velocity dispersions. Compared to Fig. 2, more data are shown because we are no longer discarding spaxels with weak H β emission that do not meet our S/N criterion.

3.3 Gas kinematic properties

Gas kinematics were derived at each spaxel using a single Gaussian fit to all emission lines simultaneously with LZIFU. Rows E and F of Fig. 1 show the fitted emission-line velocity dispersion and velocity. The velocity dispersion maps show that emission lines tend to broaden away from the disc. This broadening could be due to expanding shock fronts that are too small to spatially resolve or due to two distinct velocity components that we are unable to resolve in our spectra. The extraplanar gas is still rotating in the same sense as the disc.

Ho et al. (2016b) empirically determined criteria to differentiate edge-on galaxies dominated by large-scale winds from galaxies whose extraplanar emission is dominated by other processes such as diffuse ionized gas or satellite accretion. The criteria involve the asymmetry of the velocity field and the velocity dispersion of the extraplanar gas. Strong disk–halo interactions driven by winds do not have a perfectly symmetric velocity field (e.g. Shopbell & Bland-Hawthorn 1998; Sharp & Bland-Hawthorn 2010; Westmoquette et al. 2011). The asymmetry of the velocity field is calculated from the velocity map by reflecting the map over the galaxy major axis. A difference map is constructed by subtracting the reflected velocity from the original velocity map.

We show this difference map in row G of Fig. 1. The standard deviation of the difference maps, weighted by the error on the velocities, gives an estimate of the asymmetry between the two sides of the disc. We only use the difference maps at locations greater than one effective radius (shown as a dotted ellipse), where gas entrained in a wind is expected to be an important kinematic component. Following Ho et al. (2016b), we increase the r_e used by 1 arcsec (denoted as $\tilde{r_e}$) to reduce the effect of beam smearing. The asymmetry parameter is denoted by ξ, and is defined in equations 1 and 2 of Ho et al. (2016b), repeated here:

$$\xi = \frac{\xi_+ + \xi_-}{2}, \tag{1}$$

where

$$\xi_{+/-} = \underset{r_{+/-} > \tilde{r_e}}{\text{std}} \left(\frac{v_{\text{gas}} - v_{\text{gas,flipped}}}{\sqrt{\text{Err}(v_{\text{gas}})^2 + \text{Err}(v_{\text{gas,flipped}})^2}} \right). \tag{2}$$

The ratio of gas velocity dispersion to rotation is the second parameter used to identify wind galaxies in Ho et al. (2016b). We utilize the parameter η_{50}, the ratio of the median velocity dispersion of all spaxels outside 1 $\tilde{r_e}$ with S/N of H α $>$ 5 to the rotational velocity of the galaxy, v_{rot}. Because our SAMI observations do not have sufficient spatial coverage to probe the maximum rotational velocity, we have used the stellar mass Tully–Fisher relation of Bell & de Jong (2001) to estimate v_{rot} as in Ho et al. (2016b).

Values for the two empirical parameters ξ and η_{50} are given in Table 2 for our edge-on galaxy sample. Ho et al. (2016b) empirically classified galaxies as being wind-dominated when $\eta_{50} > 0.3$ and $\xi > 1.8$. Using these constraints, we indicate whether or not our galaxies are wind-dominated in Table 2. We were unable to classify Galaxy 6 due to the high uncertainties on the velocity dispersions at distances $>1r_e$, resulting in only two spaxels for analysis ($N_{\text{pix}} > 100$ is recommended for a robust parameter measurement). Three out of the remaining five galaxies were classified as wind dominated according to the Ho et al. (2016b) criteria. Galaxies 4

Downloaded from https://academic.oup.com/mnras/article-abstract/471/2/2438/3930853/The-SAMI-Galaxy-Survey-disc-halo-interactions-in
by California Institute of Technology user
on 21 September 2017

Table 2. Classifying winds with velocity asymmetry (ξ) and dispersion parameters (η_{50}) following Ho et al. (2016b). Galaxies are classified as 'wind-dominated' according to Ho et al. (2016b) if $\eta_{50} > 0.3$ and $\xi > 1.8$. The number of spaxels at radii greater than r_e that meet our S/N criterion is shown in column 2. Unfortunately, there is insufficient data for Galaxy 6 to perform this classification.

	GAMA ID	$N_{\rm pix}$	η_{50}	ξ	Wind
1	551202	168	0.371	3.556	Yes
2	417678	356	0.707	4.602	Yes
3	593680	283	0.415	2.182	Yes
4	600030	134	0.513	1.647	No
5	376293	221	0.455	1.43	No
6	227607	2	–	–	?

and 5 were not classified as wind-dominated, but they lie close to the classification boundary. Disc warps and flares are not expected to significantly contribute to the η_{50} and ξ parameters in these galaxies (Ho et al. 2016b). Galaxy 2 has the largest asymmetry parameter $\xi = 4.6$ which could be enhanced by a possible interaction with a nearby galaxy to the south. We note that the values of η_{50} and ξ were conservatively chosen by Ho et al. (2016b), based on a sample of 40 galaxies, in order to have a convenient separation into 'wind-dominated' and 'not wind-dominated' galaxies. The distribution of galaxy η_{50} and ξ values is not bimodal, and the wind classification is not absolute (see Tescari et al. submitted). Therefore, a galaxy with an $\eta_{50} < 0.3$ and/or $\xi < 1.8$ may still host a weaker wind.

3.4 Summary of optical diagnostic maps

Correlations between the line ratios [N II]/Hα, [S II]/Hα and [O I]/Hα and velocity dispersion have been observed in systems with galactic-wide shock activities (Rich et al. 2011; Ho et al. 2014). A positive correlation exists between the line ratios and velocity dispersions of the extraplanar gas for half of our sample. Fig. 3 shows the relation between emission-line gas σ, line ratios [N II]/Hα, [S II]/Hα and [O I]/Hα, and disc height. The spaxels bifurcate, with the disc and extraplanar regions having different σ-line ratio distributions. We expect shocked gas to have higher emission-line ratios and higher velocity dispersion than gas purely excited by star formation. Emission broadened by beam smearing alone should not have higher [N II]/Hα ratios, because the excitation is still from star formation. Furthermore, beam smearing causes increased velocity dispersions in the centre of a galaxy where the velocity gradient is steepest (Green et al. 2014). To focus on the extra-planar gas, we mask out the central $r_{\rm e}$ (padded by 1 arcsec) and measure the correspondence between σ and the line ratios [N II]/Hα and [S II]/Hα using Kendall's tau correlation coefficients (ρ) and their significance values (in the range 0–1, with smaller numbers indicating higher significance). The SCIPY.STATS package was used for spaxels that have [N II](or [S II]), Hα and σ S/N > 5 and the values of ρ and significance are included in the bottom right corners of the corresponding panels of Fig. 3.

Extraplanar gas in Galaxies 1–3, shows significant, although weak, positive correlation between the [N II]/Hα (and [S II]/Hα) line ratio and σ ($>5\sigma$), likely due to shock mixing.

Gas excited by star formation in the disks of galaxies is not expected to show a correlation between emission-line ratios and velocity dispersion.[3] For all galaxies except Galaxy 3, the disc (grey points) does not show a changing line ratio with changing velocity dispersion (i.e. line ratios and σ are not correlated). Where there is detectable extraplanar gas, these spaxels tend to show a positive correlation between line ratio, velocity dispersion and disc height.

3.5 Star-forming properties determined from optical data.

It has long been known that galaxies with higher SFR surface densities are more likely to host winds (Heckman et al. 1990, 2015; Ho et al. 2016b). However, it is difficult to conduct inter-sample studies because SFR surface densities are sensitive to the assumptions regarding the SFR tracer and the area under consideration.

SFRs from Hα were derived from SAMI data as follows. We have measured the spectrum of each galaxy in our sample within an elliptical aperture mask of 1 $\tilde{r_{\rm e}}$. The spectra from the original data cubes were binned (taking spatial covariance into account) and fitted with LZIFU, as described in Section 2.6. LZIFU removes the contribution of stellar absorption from the emission lines. The Hα emission-line flux was corrected for extinction using the Balmer decrement, Hα/Hβ, assuming the expected ratio of 2.86 for Case B recombination and a temperature of $T = 10^4$ K using the Cardelli, Clayton & Mathis (1989) extinction curve. Extinction-corrected Hα fluxes were converted to SFRs using the Kennicutt (1998) calibration.

The Ho et al. (2016b) sample consists of 40 galaxies, 15 of which were classified as wind-dominated using the kinematic criteria presented in Section 3.3. Using the same area definition as this work, Ho et al. (2016b) found that edge-on wind-dominated galaxies in the SAMI Galaxy Survey have a broad range of $\Sigma_{\rm SFR} \sim$ [0.001, 0.03) $M_\odot$ yr^{-1} kpc^{-2}. Our sample spans $\Sigma_{\rm SFR}$ of 0.007–0.05 $M_\odot$ yr^{-1} kpc^{-2}, with galaxies kinematically classified as wind-dominated having the highest SFR surface densities of our sample ($\Sigma_{\rm SFR}$ >0.015 $M_\odot$ yr^{-1} kpc^{-2}). Galaxy 4 also has a $\Sigma_{\rm SFR}$ consistent with the wind-dominated galaxies (0.044 $M_\odot$ yr^{-1} kpc^{-2}) in our sample, even though its ionized gas kinematics do not show clear signs of winds. We note that our Galaxies 2, 3 and 5 are also in the full sample of Ho et al. (2016b). Galaxies 1, 4 and 6 were not included in the analysis of Ho et al. (2016b) because they did not meet their stricter inclination criterion.

Star formation history could play an important role in the detection of winds. Authors such as Ho et al. (2016b), Sato et al. (2009) and Sharp & Bland-Hawthorn (2010) find that bursty star formation is preferred over continuous star formation for the driving of winds. Using the spectra extracted from an elliptical aperture covering the central $\tilde{r_{\rm e}}$, we also measured the $D_n(4000)$ and EW(Hδ_A) indices, which are probes of star formation history (Balogh et al. 1999; Kauffmann et al. 2003).

$D_n(4000)$ is a measurement of the amplitude of the discontinuity at 4000 Å. $D_n(4000)$ reflects the mean temperature of stars responsible for the continuum and increases as a function of age. We use the definition of Bruzual (1983), with the narrower passbands (hence the subscript n) proposed by Balogh et al. (1999) to measure $D_n(4000)$ values from our spectra. For any stellar type, the value of $D_n(4000)$ is also sensitive to stellar metal abundance, being lower for stars of lower metallicity. As a result, the $D_n(4000)$ amplitude will be affected by radial abundance gradients of galaxies. By using spectra from within one effective radius to calculate the $D_n(4000)$

[3] However, the [N II]/Hα ratio may show a correlation in the absence of shocks because it is most sensitive to metallicity and therefore is often peaked in the centre of a galaxy. Because the velocity dispersion is often also peaked at the centre of our galaxies, mostly due to beam smearing, a correlation of [N II]/Hα and σ in the disc may be expected.

Downloaded from https://academic.oup.com/mnras/article-abstract/471/2/2438/3930853/The-SAMI-Galaxy-Survey-disc-halo-interactions-in
by California Institute of Technology user
on 21 September 2017

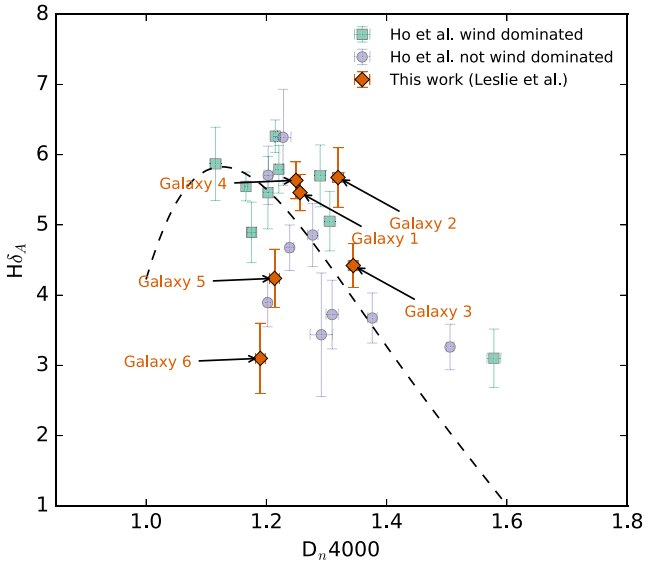

Figure 4. Star formation history traced by $D_n(4000)$ and $H\,\delta_A$ of our galaxies (orange diamonds). Comparison galaxies with $\log(\Sigma_{SFR}) > -2.4$ from Ho et al. (2016b) are also included. The wind-dominated galaxies from Ho et al. (2016b) are shown as green squares and the rest of the comparison sample as purple circles. The dashed curve indicates the median SDSS relation. Galaxies above this dashed line have 'bursty' SFHs.

values for each galaxy, we should mitigate this problem because local disc galaxies have similar metallicity gradients when calculated in terms of effective radii (Roig, Blanton & Yan 2015).

We use the method of Worthey & Ottaviani (1997) to measure the equivalent width of the $H\,\delta_A$ absorption in our 1 $\tilde{r_e}$ spectra. The subscript 'A' indicates a wide (∼40 Å) central passband is used. To account for contribution from nebular emission, we include the $H\,\delta$ emission line in our LZIFU fit and subtract the emission-line flux when the line is significant (S/N > 3). For Galaxy 6, the equivalent width was calculated by hand due to its complex line profile dominated by emission. A strong $H\,\delta$ absorption feature is usually interpreted as evidence that a burst of star formation occurred in the last Gyr (Couch & Sharples 1987).

Combining the $D_n(4000)$ and $H\,\delta_A$ indices has been employed in a simple diagnostic to distinguish between continuous and burst star formation histories (Kauffmann et al. 2003).

Ho et al. (2016b) fit a polynomial to the median relation of the star-forming galaxies in SDSS DR 7 on the $D_n(4000)$–$H\,\delta_A$ plane. Galaxies above the median $D_n(4000)$–$H\,\delta_A$ relation are more likely to have had a bursty rather than a continuous star formation history. This relation is shown in Fig. 4 along with our radio-selected sample and the two groups of galaxies in Ho et al. (2016b) with Σ_{SFR} matched to our sample ($\Sigma_{SFR} > -2.4$). The FIRST catalogue only contains galaxies with a high surface brightness, biasing our radio-selected sample towards a larger fraction of wind-dominated galaxies. For a fair comparison, we have selected galaxies from Ho et al. (2016b) with $\log(\Sigma_{SFR}) > -2.4$ to compare with our radio-selected sample. This matching results in a sample of 11 wind-dominated galaxies and 9 non-wind-dominated galaxies from the original Ho et al. (2016b) sample.

Ho et al. (2016b) found that the wind-dominated galaxies lie on average above the median $D_n(4000)$–$H\,\delta_A$ relation of the SDSS galaxies, whereas the non-wind-dominated galaxies are distributed both above and below the median. Galaxies with high EW($H\,\delta$) for a given $D_n(4000)$ value must have been observed a few hundred million years after a burst of star formation – once the emission from the A-star population begins to dominate over the O and B stars (where the Balmer absorption is not as strong). In our sample, Galaxies 1–4, with the highest Σ_{SFR} all fall above the median relation. This follows the finding of Ho et al. (2016b) that wind-dominated galaxies tend to have a bursty star formation history.

4 RADIO EMISSION

We compare the radio continuum emission measured by the FIRST survey with the optical emission-line gas ratios (specifically [N II]/H α) of our galaxies in Fig. 5. The synthesized beam size of the radio images is represented by the blue ellipses at the bottom right of the images. The typical beam size is 5.4 × 6.4.

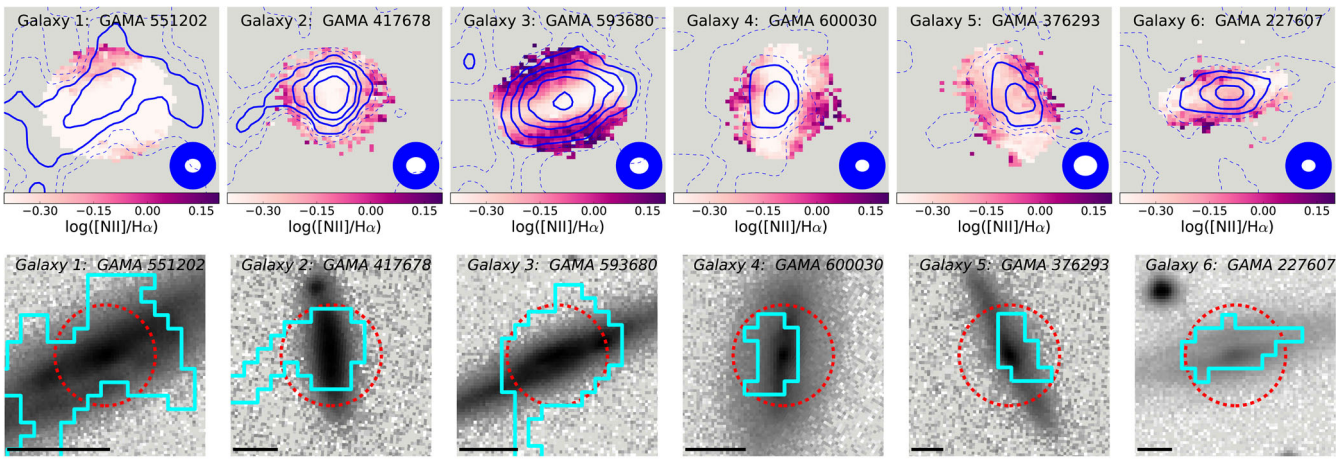

Figure 5. Top: Radio contours (blue) overlaid on the [N II]/H α map of each galaxy. Solid contours are drawn at 3, 5, 7, 10 and 15 times the rms of the FIRST images (typically 0.15 mJy). Dashed contours are drawn at 1 and 2 times the rms. A white ellipse shows the size of the optical seeing disc and the synthesized beam of the radio observations is indicated by a blue ellipse. The optical images provide data of superior angular resolution. Galaxies 1–3 have wind-dominated kinematics. Bottom: The extent of each blob fitted with the BLOBCAT algorithm of Hales et al. (2012) is outlined in cyan. Blobs encompass regions with S/N > 2. Each panel is 30 arcsec on the side. The background grey-scale map is the SDSS-*r*-band image. A black bar in the bottom left of the panels indicates 5 kpc at the redshift of each galaxy. The SAMI hexabundle field of view is indicated by a red circle.

Downloaded from https://academic.oup.com/mnras/article-abstract/471/2/2438/3930853/The-SAMI-Galaxy-Survey-disc-halo-interactions-in
by California Institute of Technology user
on 21 September 2017

Table 3. Derived properties of the six galaxies in our sample. Radio SFRs are measured using global 1.4 GHz fluxes from FIRST following (Mauch & Sadler 2007). The SFR surface densities, $SFR_{r_e}/(\pi r_e^2)$, is measured using Hα emission-line flux from within one effective radius once corrected for extinction using the Balmer decrement. $D_n(4000)$ and Hδ_A are calculated from the SAMI spectra within 1 r_e. q_{TIR} is the ratio of infrared to radio luminosity defined in equation (3). The second last column shows the 'radio extent'; this is the scaleheight at which we detect resolved minor axis radio emission in the FIRST images. For galaxies without resolved minor axis emission, we give an upper limit. Sizes are converted to kpc based on the redshift of each galaxy. R_{EST} is the ratio of the area covered by each source to the area of an unresolved Gaussian source.

	GAMA ID	FIRST flux (mJy)	FIRST rms (mJy beam^{-1})	$SFR_{1.4\,GHz}$ $M_\odot$ yr^{-1}	$\log(\Sigma_{SFR,\,H\alpha})$ $\log(M_\odot$ yr^{-1} kpc$^{-2})$	$D_n(4000)$	Hδ_A (Å)	q_{TIR}	Radio extent $\lvert z\rvert$ (kpc)	R_{EST}
1	551202	7.096	0.1558	7.1	−1.52	1.26	5.5	2.56 ± 0.03	∼4	8.93
2	417678	2.87	0.1480	2.9	−1.29	1.32	5.7	2.64 ± 0.04	∼8	1.59
3	593680	5.676	0.1453	5.7	−1.81	1.34	4.4	2.63 ± 0.03	∼5	2.42
4	600030	1.982	0.1422	2.0	−1.35	1.25	5.6	2.69 ± 0.06	<3.6	1.21
5	376293	1.260	0.1540	1.3	−2.03	1.21	4.2	2.77 ± 0.09	<5.2	0.91
6	227607	2.106	0.1535	2.1	−2.17	1.19	2.0	2.72 ± 0.04	<5.6	1.36

Contours have been drawn at 3, 5, 7, 10 and 15 times the rms of the FIRST images (typically 0.15 mJy; values for individual galaxies are tabulated in Table 3). In Table 3, we include the extent of the radio emission of the three galaxies with resolved radio emission, estimated as the maximum extent of the detected radio emission above or below the disc.

The radio emission of Galaxies 1–3 is extended along the minor axes of the galaxies at signal-to-noise levels of 2–3. These are also the three galaxies classified as 'wind-dominated' from their kinematic properties. The three wind-dominated galaxies are detected at higher signal-to-noise (by a factor of ∼3) in the radio images than Galaxies 4–6.

The minor axis radio emission is unresolved in the three galaxies not kinematically classified as wind-dominated (Galaxies 4–6). The observed size of the minor axis (from the FIRST catalogue) is given in Table 3 as an upper limit to the vertical extent of the radio emission. Because this measurement is convolved with the radio PSF, the actual size of the radio minor axis could be much smaller than the number given. The three galaxies for which we do not report resolved extended minor axis 1.4 GHz emission are at a higher redshift than those in which we do, meaning that they subtend a smaller angle on the sky. The reason that extended radio emission is not detected in these three galaxies could therefore be because the galaxies are not well resolved by the FIRST beam and hence we are unable to resolve any extended emission. In fact, if Galaxy 1 was at the redshift of Galaxies 5 or 6, we would not be able to resolve the extended emission because the beam size is >5 kpc, whereas the extended emission only reaches to ∼4 kpc above the disc.

Notes describing the emission of individual objects can be found in the Appendix.

4.1 Extended radio emission in galaxies with wind signatures

The galaxies with resolved extended radio emission (Galaxies 1–3) are the galaxies kinematically classified as wind-dominated. These galaxies have the largest $D_n(4000)$ values, implying their stellar populations are the oldest. The three galaxies also have radio 1.4 GHz SFRs greater than Hα SFRs (Table 3). Radio emission traces star formation on time-scales >10 Myr, whereas Hα emission traces star formation on time-scales <10 Myr. An older stellar population rather than a young (<10 Myr) population is more likely to be detected and extended in the radio because it takes time for the radio emission to be produced in SNe and for the CRs to be transported to the large scaleheights. Larger radio than Hα SFRs in Galaxies 1–3 are therefore consistent with a bursty star formation history.

To further investigate the extended radio emission in our sample, we use the BLOBCAT software (Hales et al. 2012), which uses the flood fill algorithm to detect and catalogue 'blobs' that represent sources in a 2D astronomical image. In particular, BLOBCAT has been designed to analyse the Stokes I intensity and linear polarization of radio-wavelength images. BLOBCAT was used to analyse 30 × 30 arcsec cut-out FIRST images of each of our six objects. We required a detection S/N (signal per pixel / rms noise in the FIRST map) of at least three[4] and blobs include connecting pixels down to 2σ flux levels. The rms values were taken from the FIRST catalogue, which gives local rms values computed by combining the measured noise from all grid pointing images contributing to the co-added map position. We set the CLEAN bias correction to 0.25 mJy as suggested by Becker et al. (1995).

The BLOBCAT region of each source is shown overlaid on SDSS *r*-band images in the bottom row of Fig. 5.

BLOBCAT returns a parameter R_{EST} that can be used to identify sources with non-Gaussian complex morphologies. R_{EST} is the ratio of the area of the detected blob to the area covered by an unresolved Gaussian blob with the same peak surface brightness (with local bandwidth smearing taken into account). This method assumes an elliptical Gaussian PSF, whose parameters are given in the header of the FIRST image. The further the value from 1, the more non-Gaussian the object is and the more extended. We list the values of R_{EST} obtained from BLOBCAT in Table 3. R_{EST} is largest for the three galaxies classified as wind-dominated, suggesting that R_{EST} could be used to identify galaxies with a potential wind in radio images. However, Galaxy 2 has an R_{EST} (1.59) similar to the non-wind-dominated Galaxies 4–6 (mean 1.16).

4.2 Infrared-radio correlation

We calculate the total infrared luminosities (TIR; 8–1000 μm) of our sample using the calibration of Galametz et al. (2013) involving 24, 100 and 160 μm data, but drawing on the WISE 22 μm emission in place of the unavailable 24 μm *Spitzer* data. The 100 and 160 μm data are from the *Herschel*-ATLAS first data release (Bourne et al. 2016; Valiante et al. 2016).

The TIR–radio correlation is parametrized by q,

$$q = \log\left(\frac{L_{TIR}}{3.75\times10^{12}\,W}\right) - \log\left(\frac{L_{1.4\,GHz}}{WHz^{-1}}\right). \quad (3)$$

[4] BLOBCAT is optimized for S/N>5 detection threshold. However, to detect Galaxies 4–6, an S/N detection threshold of 3 was required.

Downloaded from https://academic.oup.com/mnras/article-abstract/471/2/2438/3930853/The-SAMI-Galaxy-Survey-disc-halo-interactions-in
by California Institute of Technology user
on 21 September 2017

Table 4. Evidence for wind activity.

	GAMA ID	Line ratios	Kinematics	SFH	Radio size
1	551202	√	√	√	√
2	417678	√	√	√	√
3	593680	√	√	√	√
4	600030	×	×	√	×
5	376293	×	×	×	×
6	227607	×	–	×	×

Bell (2003) found for a sample of local galaxies an average $q = 2.64 \pm 0.26$. The q values of our sample are included in Table 3. We find that the three galaxies classified as wind-dominated from their kinematics have the lowest q values (mean value 2.54 ± 0.16 compared to a mean of 2.73 ± 0.04 for Galaxies 4–6). Although the q values are consistent with star-forming galaxies, a lower q-value means that the non-thermal radio synchrotron emission is dominant over the thermal infrared emission.

5 DISCUSSION

We have considered different indicators for wind activity in our galaxies from optical gas emission and kinematic diagnostics to radio morphology. Table 4 summarizes the evidence for and against dominant wind activity in each galaxy. Emission at 1.4 GHz is produced by both thermal emission and synchrotron processes. 1.4 GHz emission is expected in both thermal and CR-driven winds. Supernovae both heat the gas and accelerate the CRs. In this section, we discuss how galactic winds potentially driven by a combination of CR pressure and SNe activity can explain our observations. We then discuss future observations that could further constrain our interpretations.

Galaxies with a starburst-driven wind have ionization properties consistent with shock processes. Dopita & Sutherland (1996) found that ∼50 per cent of mechanical energy from the wind is converted into energy capable of ionizing gas. If the SAMI data are tracking material that has been entrained by a wind, then the emission lines with high line ratios are likely to be excited by shocks. A correlation between the FWHM of emission lines and shock velocity can occur when radiative shocks move into denser clouds that have a fractal distribution (Dopita et al. 2012). Further, a one-to-one correlation can be explained by the observation of two shocks moving in opposite directions (Dopita et al. 2012). Our data are unable to resolve individual shock fronts, so shocks could be propagating in any direction within an individual spaxel. As a result, one might expect the velocity dispersions would be related to the wind velocities in our sample. The maximum velocity dispersions measured (∼150 km s^{-1}) for the six galaxies in our sample are smaller than the velocity dispersions measured for galactic scale starburst-driven superwinds. However, the velocity dispersions of the six galaxies are consistent with velocity dispersions measured in the wind-dominated galaxies of Ho et al. (2016b).

CR-driven winds, as described in Booth et al. (2013), result in lower wind velocities than thermal feedback models alone. For example, simulations by Booth et al. (2013) predict an outflow velocity for a Milky Way-like galaxy of ∼200 km s^{-1} rather than the ∼1000 km s^{-1} predicted by thermal feedback models. Girichidis et al. (2016) also found that thermally driven winds are hot, mostly made of ionized hydrogen and have low densities (∼10^{-27} g cm^{-3}), whereas CR-driven winds are one to two orders of magnitude denser (∼10^{-26} to 10^{-25} g cm^{-3}), are warm (10^4K) and are composed of a mixture of atomic and molecular hydrogen. The gentle acceleration of the ISM that occurs in CR-driven outflow simulations results in multiphase winds, which include a cool component generally not present in thermally driven winds (Girichidis et al. 2016). Modelling the wind geometry to obtain a wind velocity and comparing observations of molecular and atomic hydrogen gas with the predictions of Girichidis et al. (2016) and Simpson et al. (2016) will help understand the relative importance of CRs as a wind-driving mechanism.

In localized regions of active star formation, superbubbles can locally inject a substantial amount of energy into the surroundings, allowing hot gas to reach considerable heights (de Avillez & Breitschwerdt 2004). When considering the effect of CRs, which help to push the plasma against the gravitational pull of the galaxy, even a late-type spiral can achieve a steady large-scale wind with a global mass-loss rate of ∼0.3 $M_\odot$ yr^{-1} and a low velocity of ∼10 km s^{-1} (Breitschwerdt, McKenzie & Voelk 1993). If stellar winds and supernovae are responsible for the large amounts of extraplanar gas, with chimneys being the main mode of CR and gas transport, then one might expect to see a correlation of multiple ISM tracers as they follow individual filaments. Dettmar (1992) found such a correlation between filaments of Hα and radio continuum emission features in NGC 5775. Future sensitive high-resolution radio and optical imaging will help constrain any spatial correlation on a larger sample. We observe a correlation between SFR surface density and the extent of the minor axis radio emission. Such a correlation could imply that a large amount of star formation activity is required to blow a hole in the disc.

Synchrotron protrusions from edge-on disks (Reuter et al. 1991; Seaquist & Odegard 1991) and ordered halo magnetic fields (Hummel & Dahlem 1990; Hummel et al. 1991) can also be indicative of winds. The radio emission that extends slightly in the direction of the minor axes of Galaxies 1 and 3 appear similar to the polarized intensity of galaxies such as NGC 5775, which trace the magnetic field and a possible bi-conical outflow (Duric & Seaquist 1988; Tüllmann & Dettmar 2000; Soida et al. 2011) Some synchrotron protrusions in Galaxies 1–3 are observed. Although these protrusions hint that CRs are playing an important role in the disc–halo interaction, we do not have radio data of sufficient resolution or sensitivity to answer questions about the nature of the CRs and what is driving the winds. Electrons lose energy as they propagate through synchrotron radiation and interactions with ambient photons via the inverse Compton process (Collins et al. 2000) changing the spectral index of the non-thermal emission. As such, spectral ageing (e.g. Heesen et al. 2009) could constrain the mode of CR transport (Uhlig et al. 2012). Higher resolution radio imaging of the disc at multiple frequencies will help to separate the synchrotron from thermal emission and determine the origin of the CR emission.

6 CONCLUSION

We have studied six edge-on star-forming galaxies in the SAMI Galaxy Survey that are detected in the 1.4 GHz VLA FIRST survey. These six galaxies are candidates for studying CR-driven outflows in star-forming galaxies. Shock-like emission-line ratios are found in all six objects. Significant positive correlation between velocity dispersion, [N II]/Hα ratio and disc height indicative of shocks is found for three out of six galaxies. Galaxies 1–3 are classified as wind-dominated using the gas kinematic criteria of Ho et al. (2016b). The extraplanar gas, interpreted as the outflowing component, is observed to be rotating in the same sense as the disc. This co-rotation is not surprising as the outflowing material is

Downloaded from https://academic.oup.com/mnras/article-abstract/471/2/2438/3930853/The-SAMI-Galaxy-Survey-disc-halo-interactions-in
by California Institute of Technology user
on 21 September 2017

expected to entrain part of the rotating disc material. We discuss the details of each object and speculate on likely explanations for our observations in the Appendix.

Galaxies in our sample with extended radio emission have wind-like signatures. The three galaxies in our sample with extended radio emission have bursty star formation histories, high specific SFRs and high SFR surface densities compared to the galaxies without detectable protrusions. Because these properties are indicative of starburst-driven winds, our observations imply that star formation, CR emission and outflows are intimately related.

Work is still required to understand winds in star-forming galaxies both theoretically and observationally. CRs could help explain the presence of winds and high mass-loading factors in some galaxies. However, the relative importance of CR processes is still unconstrained because extraplanar gas is diffuse and difficult to observe. The comparison of IFU data to future deep radio observations with high angular resolution and covering a range of frequencies will allow us to observationally determine how common CR-driven winds are in the Universe and their relative importance in transporting material into galaxy haloes.

ACKNOWLEDGEMENTS

This research was conducted by the Australian Research Council Centre of Excellence for All-sky Astrophysics (CAASTRO), through project number CE110001020.

The SAMI Galaxy Survey is based on observations made at the Anglo-Australian Telescope. The Sydney-AAO Multi-object Integral field spectrograph (SAMI) was developed jointly by the University of Sydney and the Australian Astronomical Observatory. The SAMI input catalogue is based on data taken from the SDSS, the GAMA Survey and the VST ATLAS Survey. The SAMI Galaxy Survey is funded CAASTRO and other participating institutions. The SAMI Galaxy Survey website is http://sami-survey.org/.

GAMA is a joint European-Australasian project based around a spectroscopic campaign using the Anglo-Australian Telescope. The GAMA input catalogue is based on data taken from the Sloan Digital Sky Survey and the UKIRT Infrared Deep Sky Survey. Complementary imaging of the GAMA regions is being obtained by a number of independent survey programmes including *GALEX* MIS, VST KiDS, VISTA VIKING, WISE, *Herschel*-ATLAS, GMRT and ASKAP providing UV to radio coverage. GAMA is funded by the STFC (UK), the ARC (Australia), the AAO and the participating institutions. The GAMA website is http://www.gama-survey.org/.

Support for AMM is provided by NASA through Hubble Fellowship grant #HST-HF2-51377 awarded by the Space Telescope Science Institute, which is operated by the Association of Universities for Research in Astronomy, Inc., for NASA, under contract NAS5-26555. JTA acknowledges the award of a SIEF John Stocker Fellowship. MSO acknowledges the funding support from the Australian Research Council through a Future Fellowship (FT140100255). SB acknowledges the funding support from the Australian Research Council through a Future Fellowship (FT140101166).

REFERENCES

Allen M. G., Groves B. A., Dopita M. A., Sutherland R. S., Kewley L. J., 2008, ApJS, 178, 20
Allen J. T. et al., 2015, MNRAS, 446, 1567
Axon D. J., Taylor K., 1978, Nature, 274, 37
Baldwin J. A., Phillips M. M., Terlevich R., 1981, PASP, 93, 5
Balogh M. L., Morris S. L., Yee H. K. C., Carlberg R. G., Ellingson E., 1999, ApJ, 527, 54
Becker R. H., White R. L., Helfand D. J., 1995, ApJ, 450, 559
Belfiore F. et al., 2016, MNRAS, 461, 3111
Bell E. F., 2003, ApJ, 586, 794
Bell E. F., de Jong R. S., 2001, ApJ, 550, 212
Beuermann K., Kanbach G., Berkhuijsen E. M., 1985, A&A, 153, 17
Blanc G. A., Heiderman A., Gebhardt K., Evans N. J., II, Adams J., 2009, ApJ, 704, 842
Bland J., Tully B., 1988, Nature, 334, 43
Bland-Hawthorn J., Freeman K. C., Quinn P. J., 1997, ApJ, 490, 143
Bland-Hawthorn J. et al., 2011, Opt. Express, 19, 2649
Bloemen H., Duric N., Irwin J., 1993, in Leahy D. A., Hicks R. B., Venkatesan D., eds, Int. Cosmic Ray Conf. Vol. 2, New Insights into Cosmic-Ray Origin and Propagation from High-Resolution Radio Imaging of the Edge-on Galaxy NGC 3556. World Scientific Press, Singapore, p. 279
Booth C. M., Agertz O., Kravtsov A. V., Gnedin N. Y., 2013, ApJ, 777, L16
Bourne N. et al., 2016, MNRAS, 462, 1714
Breitschwerdt D., McKenzie J. F., Voelk H. J., 1993, A&A, 269, 54
Bruzual A. G., 1983, ApJ, 273, 105
Bryant J. J., O'Byrne J. W., Bland-Hawthorn J., Leon-Saval S. G., 2011, MNRAS, 415, 2173
Bryant J. J., Bland-Hawthorn J., Fogarty L. M. R., Lawrence J. S., Croom S. M., 2014, MNRAS, 438, 869
Bryant J. J. et al., 2015, MNRAS, 447, 2857
Cappellari M., Emsellem E., 2004, PASP, 116, 138
Cardelli J. A., Clayton G. C., Mathis J. S., 1989, ApJ, 345, 245
Cole S., Lacey C. G., Baugh C. M., Frenk C. S., 2000, MNRAS, 319, 168
Collins J. A., Rand R. J., Duric N., Walterbos R. A. M., 2000, ApJ, 536, 645
Condon J. J., 1992, ARA&A, 30, 575
Condon J. J., Cotton W. D., Greisen E. W., Yin Q. F., Perley R. A., Taylor G. B., Broderick J. J., 1998, AJ, 115, 1693
Couch W. J., Sharples R. M., 1987, MNRAS, 229, 423
Croom S. M. et al., 2012, MNRAS, 421, 872
de Avillez M. A., Breitschwerdt D., 2004, A&A, 425, 899
Denicoló G., Terlevich R., Terlevich E., 2002, MNRAS, 330, 69
Dettmar R. J., 1992, Fundam. Cosm. Phys., 15, 143
Domgorgen H., Mathis J. S., 1994, ApJ, 428, 647
Dopita M. A., Sutherland R. S., 1996, ApJS, 102, 161
Dopita M. A., Payne J. L., Filipović M. D., Pannuti T. G., 2012, MNRAS, 427, 956
Driver S. P. et al., 2011, MNRAS, 413, 971
Duric N., Seaquist E. R., 1988, ApJ, 326, 574
Duric N., Irwin J., Bloemen H., 1998, A&A, 331, 428
Everett J. E., Zweibel E. G., Benjamin R. A., McCammon D., Rocks L., Gallagher J. S., III, 2008, ApJ, 674, 258
Farage C. L., McGregor P. J., Dopita M. A., Bicknell G. V., 2010, ApJ, 724, 267
Fogarty L. M. R. et al., 2012, ApJ, 761, 169
Galametz M. et al., 2013, MNRAS, 431, 1956
Genzel R. et al., 2011, ApJ, 733, 101
Genzel R. et al., 2014, ApJ, 796, 7
Girichidis P. et al., 2016, ApJ, 816, L19
González Delgado R. M., Cerviño M., Martins L. P., Leitherer C., Hauschildt P. H., 2005, MNRAS, 357, 945
Green A. W. et al., 2014, MNRAS, 437, 1070
Grimes J. P. et al., 2009, ApJS, 181, 272
Haffner L. M. et al., 2009, Rev. Mod. Phys., 81, 969
Hales C. A., Murphy T., Curran J. R., Middelberg E., Gaensler B. M., Norris R. P., 2012, MNRAS, 425, 979
Hartquist T. W., Morfill G. E., 1986, ApJ, 311, 518
Heckman T. M., Armus L., Miley G. K., 1990, ApJS, 74, 833
Heckman T. M., Alexandroff R. M., Borthakur S., Overzier R., Leitherer C., 2015, ApJ, 809, 147
Heesen V., Beck R., Krause M., Dettmar R.-J., 2009, A&A, 494, 563
Ho I.-T. et al., 2014, MNRAS, 444, 3894
Ho I.-T. et al., 2016a, Ap&SS, 361, 280

Downloaded from https://academic.oup.com/mnras/article-abstract/471/2/2438/3930853/The-SAMI-Galaxy-Survey-disc-halo-interactions-in
by California Institute of Technology user
on 21 September 2017

Ho I.-T. et al., 2016b, MNRAS, 457, 1257
Hoopes C. G., Walterbos R. A. M., 2003, ApJ, 586, 902
Hopkins A. M. et al., 2013, MNRAS, 430, 2047
Hubble E. P., 1926, ApJ, 64, 321
Hummel E., Dahlem M., 1990, in Beck R., Wielebinski R., Kronberg P. P., eds, Proc. IAU Symp. 140, Galactic and Intergalactic Magnetic Fields. Kluwer, Dordrecht, p. 219
Hummel E., van Gorkom J. H., Kotanyi C. G., 1983, ApJ, 267, L5
Hummel E., Beck R., Dahlem M., 1991, A&A, 248, 23
Irwin J. A., Madden S. C., 2006, A&A, 445, 123
Ivezić Ž. et al., 2002, AJ, 124, 2364
Kauffmann G. et al., 2003, MNRAS, 346, 1055
Kelvin L. S. et al., 2012, MNRAS, 421, 1007
Kennicutt R. C., Jr, 1998, ARA&A, 36, 189
Kereš D., Katz N., Davé R., Fardal M., Weinberg D. H., 2009, MNRAS, 396, 2332
Kewley L. J., Dopita M. A., 2002, ApJS, 142, 35
Kewley L. J., Ellison S. L., 2008, ApJ, 681, 1183
Kewley L. J., Dopita M. A., Sutherland R. S., Heisler C. A., Trevena J., 2001, ApJ, 556, 121
Kewley L. J., Groves B., Kauffmann G., Heckman T., 2006, MNRAS, 372, 961
Krause M., 2012, in Soida M. et al., eds, Magnetic Fields in the Universe III - From Laboratory and Stars to Primordial Structures. Jagiellonian University, Astronomical Observatory, p. 155
Liske J. et al., 2015, MNRAS, 452, 2087
Madsen G. J., Reynolds R. J., 2005, ApJ, 630, 925
Markwardt C. B., 2009, in Bohlender D. A., Durand D., Dowler P., eds, ASP Conf. Ser. Vol. 411, Astronomical Data Analysis Software and Systems XVIII. Astron. Soc. Pac., San Francisco, p. 251
Mauch T., Sadler E. M., 2007, MNRAS, 375, 931
Miller S. T., Veilleux S., 2003, ApJ, 592, 79
Monreal-Ibero A., Arribas S., Colina L., 2006, ApJ, 637, 138
Newman S. F. et al., 2012, ApJ, 761, 43
Norman C. A., Ikeuchi S., 1989, ApJ, 345, 372
Normandeau M., Taylor A. R., Dewdney P. E., 1996, Nature, 380, 687
Oey M. S. et al., 2007, ApJ, 661, 801
Otte B., Dettmar R.-J., 1999, A&A, 343, 705
Owers M. S. et al., 2017, MNRAS, 468, 1824
Parker E. N., 1992, ApJ, 401, 137
Pettini M., Pagel B. E. J., 2004, MNRAS, 348, L59
Pettini M., Steidel C. C., Adelberger K. L., Dickinson M., Giavalisco M., 2000, ApJ, 528, 96
Pietz J., Kerp J., Kalberla P. M. W., Mebold U., Burton W. B., Hartmann D., 1996, A&A, 308, L37
Popescu C. C., Tuffs R. J., Kylafis N. D., Madore B. F., 2004, A&A, 414, 45
Rand R. J., 1998, ApJ, 501, 137
Reuter H.-P., Krause M., Wielebinski R., Lesch H., 1991, A&A, 248, 12
Reynolds R. J., 1993, in Holt S. S., Verter F., eds, AIP Conf. Proc. Vol. 278, Back to the Galaxy. Am. Inst. Phys., New York, p. 156
Rich J. A., Dopita M. A., Kewley L. J., Rupke D. S. N., 2010, ApJ, 721, 505
Rich J. A., Kewley L. J., Dopita M. A., 2011, ApJ, 734, 87
Robotham A. S. G. et al., 2011, MNRAS, 416, 2640
Roig B., Blanton M. R., Yan R., 2015, ApJ, 808, 26
Rossa J., Dettmar R.-J., 2000, A&A, 359, 433
Rossa J., Dettmar R.-J., 2003, A&A, 406, 493
Ruszkowski M., Yang H.-Y. K., Zweibel E., 2017, ApJ, 834, 208
Sadler E. M. et al., 2002, MNRAS, 329, 227
Salem M., Bryan G. L., 2014, MNRAS, 437, 3312
Sato T., Martin C. L., Noeske K. G., Koo D. C., Lotz J. M., 2009, ApJ, 696, 214
Seaquist E. R., Odegard N., 1991, ApJ, 369, 320
Shapiro P. R., Field G. B., 1976, ApJ, 205, 762
Sharp R. G., Bland-Hawthorn J., 2010, ApJ, 711, 818
Sharp R. et al., 2006, in McLean I. S., Iye M., eds, Proc. SPIE Conf. Ser. Vol. 6269, Ground-based and Airborne Instrumentation for Astronomy. SPIE, Bellingham, p. 62690G
Sharp R. et al., 2015, MNRAS, 446, 1551
Shopbell P. L., Bland-Hawthorn J., 1998, ApJ, 493, 129
Shull J. M., McKee C. F., 1979, ApJ, 227, 131
Simpson C. M., Pakmor R., Marinacci F., Pfrommer C., Springel V., Glover S. C. O., Clark P. C., Smith R. J., 2016, ApJ, 827, L29
Slavin J. D., Shull J. M., Begelman M. C., 1993, ApJ, 407, 83
Smolčić V., 2009, ApJ, 699, L43
Soida M., Krause M., Dettmar R.-J., Urbanik M., 2011, A&A, 531, A127
Sorathia B., 1994, Master's thesis, Queen's Univ. Canada
Soto K. T., Martin C. L., 2012, ApJS, 203, 3
Soto K. T., Martin C. L., Prescott M. K. M., Armus L., 2012, ApJ, 757, 86
Springel V., Hernquist L., 2003, MNRAS, 339, 289
Steidel C. C., Erb D. K., Shapley A. E., Pettini M., Reddy N., Bogosavljević M., Rudie G. C., Rakic O., 2010, ApJ, 717, 289
Stoughton C. et al., 2002, AJ, 123, 485
Taylor E. N. et al., 2011, MNRAS, 418, 1587
Tüllmann R., Dettmar R.-J., 2000, A&A, 362, 119
Tumlinson J. et al., 2011, Science, 334, 948
Uhlig M., Pfrommer C., Sharma M., Nath B. B., Enßlin T. A., Springel V., 2012, MNRAS, 423, 2374
Valiante E. et al., 2016, MNRAS, 462, 3146
Veilleux S., Osterbrock D. E., 1987, ApJS, 63, 295
Veilleux S., Rupke D. S., 2002, ApJ, 565, L63
Veilleux S., Cecil G., Bland-Hawthorn J., 1995, ApJ, 445, 152
Veilleux S., Shopbell P. L., Rupke D. S., Bland-Hawthorn J., Cecil G., 2003, AJ, 126, 2185
Veilleux S., Cecil G., Bland-Hawthorn J., 2005, ARA&A, 43, 769
Werk J. K., Prochaska J. X., Thom C., Tumlinson J., Tripp T. M., O'Meara J. M., Peeples M. S., 2013, ApJS, 204, 17
Westmoquette M. S., Smith L. J., Gallagher J. S., III, 2011, MNRAS, 414, 3719
Wiener J., Pfrommer C., Oh S. P., 2017, MNRAS, 467, 906
Worthey G., Ottaviani D. L., 1997, ApJS, 111, 377
York D. G. et al., 2000, AJ, 120, 1579

APPENDIX A: NOTES ON INDIVIDUAL OBJECTS

A1 GAMA 551202

Although only the central regions (±2.5 kpc) of GAMA 551202 are probed with SAMI, evidence for increased velocity dispersion and emission-line ratios above and below the disc is seen, particularly north of the disc away from the dust lane. GAMA 551202 is the least massive galaxy in the sample, but its $D_n(4000)$ and $H\delta_A$ values ($H\delta_A \sim 0.47$ Å above the median relation) indicate that a burst of star formation could have occurred in the past 1 Gyr. GAMA 551202 is the nearest galaxy in our sample and its large angular size allows us to resolve the extraplanar radio emission. This galaxy has extended radio emission that is offset from the optical brightness profile (position angles differ by 30 deg). Fingers of radio emission can be seen perpendicular to the disc of GAMA 551202 out to 4 kpc. It is possible that the extended radio emission is evidence for CR-driven winds (or at least the presence of a galactic wind or chimney). The optical emission-line ratios for this galaxy show that both star formation and shocks are likely contributing to the emission. It is possible that a low-velocity CR-driven wind ($\ll$100 km s^{-1}) is present in GAMA 551202, but more observations are required to confirm this.

A2 GAMA 417678

GAMA 417678 is the most extreme galaxy in the sample, having the highest optical SFR and Σ_{SFR} as well as the highest η_{50} and ξ kinematic parameters. GAMA 417678 is likely to have experienced

Downloaded from https://academic.oup.com/mnras/article-abstract/471/2/2438/3930853/The-SAMI-Galaxy-Survey-disc-halo-interactions-in
by California Institute of Technology user
on 21 September 2017

a recent burst of star formation because it lies well above the median SDSS relation in the $D_n(4000)$–H δ_A plane. GAMA 417678 is in a close pair (with GAMA 417676, $M_\star = 10^{9.98}$ $M_\odot$). Given the close proximity to another massive galaxy, a recent burst of star formation resulting from an interaction is likely for GAMA 417678. An interaction could also be the reason for the relatively large velocity dispersions (of $\sim$100 km s^{-1}) observed in the galaxy disc. One of the most noticeable features of the radio emission from GAMA 417678 is a strong ($>3\times$ rms) tail extending $\sim$7.5 kpc to the south-east. This tail is not in the direction of any neighbouring galaxies, so it is possible that the tail may be a result of a starburst-driven galactic wind that has blown a hole in the disc, allowing CRs to be advected into the halo. However, we cannot rule out the possibility that the tail is a tidal feature. The tail could also be a weak radio jet. If this were a jet, GAMA 417678 would be a rare galaxy that has high SF activity and a large-scale radio jet. Most local radio galaxies are early type objects with red colours (Smolčić 2009).

A3 GAMA 593680

GAMA 593680 shows extended radio emission reaching to heights of $\sim$5 kpc above the disc. Furthermore, the [S II]/[N II] line ratio map shows evidence of a bipolar outflow, likely a result of a supernova-driven wind. Like the other wind-dominated galaxies, GAMA 593680 lies above the median $D_n(4000)$–H δ_A relation of SDSS star-forming galaxies (by 0.47 Å). GAMA 593680 has the largest $D_n(4000)$ value, implying it has the oldest stellar populations. The strong increase of emission-line ratio with disc height ([S II]/H α increases by $\sim$0.2 dex parsec^{-1}) argues against the line ratios being caused by AGN activity and supports the idea that shocked gas is being expelled from the galaxy in a starburst-driven galactic wind, likely aided by CR pressure. The radio emission is strongly centred on the nucleus of GAMA 593680. This could be due to the high concentration of on-going star formation in the centre of the galaxy. GAMA 593680 has no obvious nearby companions, but it is the centre of a small group of small galaxies (GAMA group catalogue; Robotham et al. 2011). Although the extraplanar radio emission is close to the noise level, extended emission similar to the structure seen in GAMA 551202 can be inferred from the FIRST image out to disc heights of $\sim$5 kpc.

A4 GAMA 600030

Clumps of H α emission are seen to the north and south of the nucleus of GAMA 600030, which are not present in the optical continuum nor radio continuum emission.

GAMA 600030 shares some properties with the galaxies that have extended radio emission – it has high sSFR and high $\Sigma_{\rm SFR}$. On the other hand, its radio emission is only 40 per cent of that expected from the H α SFR and the emission was not spatially resolved in the FIRST images. It is possible that this galaxy does not have a strong CR-pressure component, due to a lack of strong magnetic field. The large SFR surface density (0.044 $M_\odot$ yr^{-1} kpc^{-2}) could drive a thermal outflow, raising the velocity dispersion (from 50 to 150 km s^{-1}) while producing shocks as the outflowing gas collides with its surroundings thereby raising the emission-line ratios.

GAMA 600030 has the second highest SFR and has a σ map very similar to that of GAMA 417678. GAMA 600030 could be wind dominated. GAMA 600030 lies above (0.58 Å) the median SDSS $D_n(4000)$–H δ_A relation. It is therefore plausible that this galaxy is experiencing a starburst-driven (radiation pressure and/or CR-driven) wind. There is an interesting region of low [S II]/[N II] ratio south of the nucleus of this galaxy. This region coincides with a knot of bright H α emission and could be a signature of a wind-blown superbubble, although high-resolution, multiwavelength observations are required to test this hypothesis.

A5 GAMA 376293

GAMA 376293 is an isolated galaxy with a knot of star formation on the south-west side of its disc seen in both the H α and optical continuum images. This region also corresponds to a region where there is a possible extraplanar clump of radio emission at $2\times$ the background rms. GAMA 376293 lies on the boundary of being classified as wind-dominated or not wind-dominated. Based on the gas kinematic classification of Ho et al. (2016b), GAMA 376293 has the high ratio of velocity dispersion-to-rotational velocity expected for a wind-dominated galaxy but its velocity field is too symmetrical. Given that galaxies with CR-driven winds have not been well studied observationally, it is possible that they result in more symmetrical velocity fields than thermal winds. The velocity dispersion of the emission-line gas of GAMA 376293 is largest in the nucleus of the disc and above and below the disc, where the emission line ratios are enhanced. This spatial correlation is in support of a galactic wind in GAMA 376293. The central spectrum of GAMA 376293 has H δ_A values lower than expected for its $D_n(4000)$ given the median SDSS relation. Ho et al. (2016b) found that galaxies below the median relation tend to not be wind-dominated. Therefore, the low H δ_A value may be further evidence against a galactic wind.

A6 GAMA 227607

GAMA 227607 is the most massive galaxy in our sample with a clear bulge and dust lane. GAMA 227607 is the most difficult candidate in which to find a wind because of the low S/N spectra obtained with SAMI away from the disc. No evidence is seen for extended radio continuum emission (down to 0.3 mJy), expected if CRs were aiding the driving of gas into the halo. The galaxy does show a biconical [N II]/H α emission line ratio map and composite spectra that could reflect a contribution from shocks. The [O III]/H β ratio is not typical of Seyfert emission, but is consistent with slow shocks (e.g. Rich et al. 2011). GAMA 227607 is in a group with another star-forming disc galaxy (GAMA 227619) with stellar mass $10^{10.59}$ $M_\odot$, located south-east of GAMA 227607. An interaction with GAMA 227619 could explain the region of high velocity dispersion gas ($\sigma = 140$ km s^{-1}) to the west of the disc in GAMA 227607. The radio emission of GAMA 227607 is concentrated along the galaxy disc and is likely to be associated with star formation activity. It is possible that GAMA 227607 hosts a weak galactic wind, but it is perhaps more likely that the enhanced emission-line ratios seen are a result of diffuse ionized gas.

This paper has been typeset from a TEX/LATEX file prepared by the author.

Downloaded from https://academic.oup.com/mnras/article-abstract/471/2/2438/3930853/The-SAMI-Galaxy-Survey-disc-halo-interactions-in
by California Institute of Technology user
on 21 September 2017